Unraveling Ce3+ detection at the surface of ceria nanopowders by UPS analysis

L. Cardenas, C. Molinet-Chinaglia, S. Loridant

Unraveling the Ce^{3+} detection at the surface of ceria nanopowders by UPS analysis

Received 00th January 20xx,
Accepted 00th January 20xx

DOI: 10.1039/x0xx00000x

Luis Cardenas*, Clément Molinet, and Stéphane Loridant*

A sequential analysis using Ultra-Violet Photoelectron Spectroscopy (UPS) and X-ray Photoelectron Spectroscopy (XPS) on ceria nanopowders has been implemented to identify the influence of the X-ray beam on the surface of this oxide. For the first time, the UPS analysis evidenced the photoreductive effect of XPS analysis on ceria after an oxidative *in situ* pretreatment, leading to an overestimation of the Ce^{3+}/Ce^{4+} ratio obtained by XPS. Based on this spectroscopy methodology, UPS imposes itself as a leading technique for analyzing powders with minimal impact on the authentic chemical state, thus paving the way for identifying the real ratio of Ce^{4+} and Ce^{3+} of ceria after oxidative and reductive *in situ* treatments.

Introduction

In the last decades, the electronic properties of ceria have been investigated, particularly the relationships between stoichiometric CeO_2 and sub-stoichiometric $CeO_{2-\delta}$, which play a central role in controlling the catalytic activity in different relevant processes.[1] In particular, Ce^{3+} cations present in $CeO_{2-\delta}$ act as a reservoir of electrons to mediate the reduction of O_2 molecules during a catalytic redox reaction, associated with high anionic mobility. The Ce^{3+}/Ce^{4+} redox couple provides exceptional oxygen storage capacity to ceria. However, this redox couple is widely impacted by the surface area.[2] This catalyst has been characterized through X-ray Photoelectron Spectroscopy (XPS), particularly the Ce^{3+}/Ce^{4+} ratio, making XPS the workhorse in the semi-quantitative determination of chemical states at the surface of ceria.[3] Although XPS provides access to elemental chemical composition and high surface sensitivity with an inelastic mean free-path (IMFP) for CeO_2 located between 2.1 nm and 6.3 nm for 1.3 KeV (close to Al kα energy = 1486.6 eV) and 5.1 KeV of incident energy, respectively.[4]

The fitting procedure of the Ce 3d core level requires more than ten components,[5] including different symmetric and asymmetric fit functions,[6] rendering the Ce 3d core level challenging to interpret and quantify. These technical and analytical aspects are at the center of the debate that still exists about the origin and determination of the Ce^{3+}/Ce^{4+} ratio states by XPS. Furthermore, standard X-ray sources (Al Kα and Mg Kα) used in XPS lab setups emit photons with energies of 1486.6 eV and 1253.6 eV, respectively. Under these conditions, photoreduction effects (photolysis) cannot be excluded, especially at the surface of ceria where Ce^{3+} is preferentially formed.[4]

The literature has reported several cases related to photolysis effects during XPS and X-ray Absorption Near-edge Spectroscopy XANES analysis. For instance, Paparazzo *et al.*,[7,8] revealed the reductive character of ceria during an XPS analysis by highlighting a change in the Ce 3d profile as a function of the X-ray exposure time. Subsequently, El Fallah *et al.*,[9] showed by XPS the different experimental parameters involved in Ce^{3+} cations formation, as surface treatments and X-ray damage induced during XPS analysis. The debate on the origin of Ce^{3+} during XPS analysis was brought back by Park *et al.*,[10] attributing Ce^{3+} enhancement to photolysis of the amorphous cerium oxide in cerium-alumina catalysts. Zhang *et al.*,[11] dealt with the photolysis issue on ceria by combining XPS and XANES. The authors found significant discrepancies between both analyses on ceria nanoparticles, showing a significantly higher concentration of Ce^{3+} by XPS analysis than that obtained by XANES in both transmission and fluorescence operating modes, a discrepancy probably caused by the X-radiation. Indeed, Wu *et al.*,[12] reported the reduction of ceria during XANES analysis with a photon energy of 7 KeV. In this work, the Ce^{3+} cations were followed using the Ce *L_3-edge* as a function of the exposure time to X-rays.

Foresee a multi-technique approach is an avenue to be explored to determine the real chemical state of many oxides and photosensitive samples, particularly the ceria Ce^{3+}/Ce^{4+} ratio. However, to date, the multi-technique implementation of certain laboratory spectroscopies (RAMAN, UV-VIS, XPS, IR) has not allowed reaching a consensus in evaluating the chemical state at the surface of stochiometric and sub-stochiometric ceria. For instance, optical UV-Vis and Raman spectroscopies have been intensively used to characterize ceria.[13] Particularly Raman spectroscopy,[14] Raman electronic scattering of Ce^{3+} cations can be combined with Raman vibrational scattering to characterize the chemical bonds of ceria. However, Raman spectroscopy is a bulk technique compared to UP spectroscopy, even if surface species such as carbonates, peroxo, and OH groups can be observed.

Univ Lyon, Université Claude Bernard-Lyon 1, CNRS, IRCELYON-UMR 5256, 2 av. A. Einstein, F-69626 Villeurbanne Cedex, France. Corresponding authors: luis.cardenas@ircelyon.univ-lyon1.fr, stephane.loridant@ircelyon.univ-lyon1.fr

† Footnotes relating to the title and/or authors should appear here.
Electronic Supplementary Information (ESI) available: [details of any supplementary information available should be included here]. See DOI: 10.1039/x0xx00000x

Furthermore, only semi-quantitative measurements can be obtained by Raman spectroscopy, and the photolysis process can be observed.[15] Photolysis effects can only be minimized by using an expensive violet laser and detection system in UV Raman mode. Finally, UV-Vis spectroscopy has also limitations since broad bands are observed, limiting a fine distinction between different electronic transitions. In parallel, further efforts have been made using synchrotron facilities to determine the Ce^{3+}/Ce^{4+} ratio. However, extreme caution is required when soft and hard X-ray sources are combined as the impact of the beam received on the surface per unit area (*power density =ϕ(hc/λ), where ϕ is the photon flux*) leads to photoreduction beam damage. To bypass this potential photoreductive effect and increase the surface sensitivity, a combined approach of low (UPS) and soft energies (XPS or RESPES at 121.5 eV and 124.5 eV) spectroscopies techniques is required to confirm the absence of the photolysis effect, allowing thus to reveal the real electronic state of the ceria. Indeed, whatever spectroscopic method is used should emphasize three factors: (i) surface preparation, (ii) mean depth resolution/excitation energy, and (iii) photon power density.

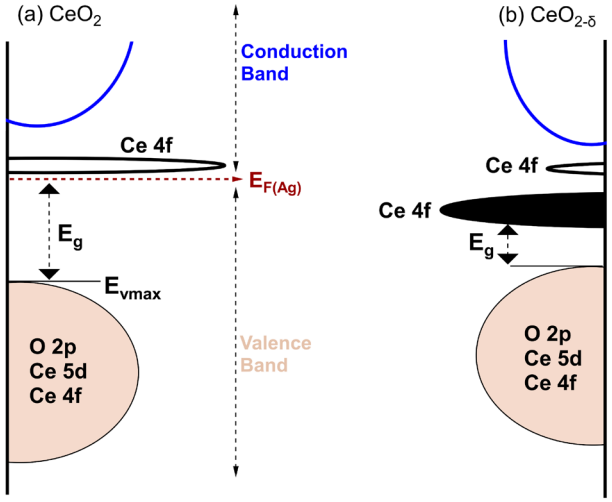

Fig. 1: Schematic diagram of the electronic structure of: (a) CeO_2 and (b) $CeO_{2-\delta}$. The dashed red line corresponds to the Fermi level of Ag foil. The Ce 4f state arises in the occupied gap (valence band) (Eg) of $CeO_{2-\delta}$.

In this context, to characterize the electronic structure of a catalytic relevant material as ceria nanopowders is essential to reveal the nature of the active sites and redox mechanisms guided by the Ce^{3+}/Ce^{4+} ratio. For instance, a high electron occupancy in the gap Ce 4f1 (Ce^{3+}) results in the deviation of stoichiometric CeO_2 (Figure 1).[16,17] The reducibility of CeO_2 is facilitated by the electron transition (occupied) O 2p → (unoccupied) Ce 5d and Ce 4f [18] concomitants with the release of two electrons from O^{2-} anions, leading to the formation of two Ce^{3+} cations. The ionic character of ceria foresees a low degree of hybridization between Ce 5d, O 2p, and Ce 4f occupied states. In this context, DFT calculations forecast a valence band formed mainly by the O 2p state with low electronic occupancy of Ce 4f and Ce 5d orbitals in the region occupied by O 2p orbitals. An extremely low density of electron tails characterizes this occupancy (Ce 4f, Ce 5d) which surrounds the interstitial region between O and Ce atoms represented by nonoverlapping muffin-tin spheres.[19]

In stoichiometric ceria (CeO_2), the low relative energy between occupied O 2p and unoccupied 4f states may render this transition sensitive to photolysis, which may induce the presence of the Ce 4f state in the valence band. In this context, UPS analysis would be a spectroscopic method intended to identify Ce 4f, especially by de-correlating its detection of undesirable effects such as photolysis and keeping a high surface sensitivity.

In this paper, we propose studying the electronic structure of ceria nanopowders to address the debate on the origin of Ce^{3+} cations. This is remediated by combining two spectroscopic technics with different mean depth resolutions, such as XPS and UPS. Simultaneously, we established a strategy using UPS as a spectroscopic reference method to pinpoint the true Ce^{3+} chemical state at the outermost surface of stochiometric and sub-stochiometric ceria in nanopowder form, especially bypassing undesirable photolysis phenomena like those observed during an XPS analysis. Furthermore, we followed the evolution of the Ce^{3+}/Ce^{4+} ratio by using Ce 4f, O 2p, and Ce 3d states after oxidative and reductive *in situ* treatments to estimate the reducibility degree of ceria ranging from shallower (UPS) to deeper layers (XPS). To adequately describe the electronic structure of stoichiometric CeO_2, an oxidizing *in situ* treatment was required previously for the UPS analysis. It has two purposes: (i) remove organic impurities and (ii) fully oxidize ceria to render it nearly stoichiometric. *In situ* oxidized ceria was analyzed according to a sequence starting with UPS at low energy (21.2 eV) followed by XPS (1486.6 eV) to determine the X-ray beam influence on the sample. Therefore keeping the UPS→XPS sequence was essential to analyze the effect of photolysis on ceria due to the high energy and power density photon flux of X-rays.

Experimental section

Materials and methods:

Ceria nanopowder in colloidal solution: An aqueous solution (10 wt% in 100 ml of water) of pure ceria (Aldrich, ref. 643009, 99.99%, particle size below 25 nm) was used as a precursor. It was ultrasonically dispersed and deposited at RT by drop-casting on Ag foil previously cleaned. This CeO_2/Ag sample was immediately introduced under vacuum, inducing thus a rapid drying of the solution.

Ceria foil model system intended to identify the Ce 3d core level transitions during *in situ* oxidation: A foil of pure ceria (Aldrich, ref. GF63193013, 99.9%) was used to obtain the spectra of Ce 3d under *in situ* conditions from full reduced to nearly stoichiometric CeO_2. The sample was exposed to Ar^+ sputtering for 6 hours at 3 KeV under vacuum. This erosion method turned the surface of the ceria into nearly reduced ceria (Ce^{3+}). Subsequently, this surface was exposed to a leak of oxygen (O_2) P≈10^{-6} Torr during XPS analysis, thus providing a clear view of the evolution of each of the components during *in situ* oxidation (Figure 2(a)).

Oxidation and reduction of colloidal solution of ceria

$CeO_{2-\delta}$ nanopowder on Ag was oxidized/reduced *in situ* using a catalytic reactor cell connected *in situ* to the PES analysis chamber under UHV, providing a direct sample transfer without contact with the air. The oxidation treatment of $CeO_{2-\delta}$/Ag was carried out under 50 mL.min^{-1} O_2 flow during 4 h at 600 °C and subsequently analyzed by UPS-XPS. In contrast, the reduction process was carried out on the sample under UHV for 4 h held at 600 °C.

Ultraviolet Photoelectron Spectroscopy

UPS analysis was used to determine the electronic structure of the valence band of ceria nanopowders. *Prior* to measurements, Ag foil was cleaned by several cycles of 2 KeV Ar^+ sputtering at RT. Then, several drops were deposited on the conducting Ag foil. This methodology for UPS sample preparation was described by Maheu et *al.*,[20] thus minimizing the charging effects during Photoelectron Spectroscopy (PES) analysis and providing a straightforward calibration *via* an absolute measurement of the Fermi level of Ag pristine foil (Figure 3). XPS and UPS spectra obtained from Ag foil after sputtering confirm the metallic character of Ag by the presence of plasmons in the Ag 3d core level, the near-absence of oxygen, and the step the Fermi in the valence band, respectively (Figure S1).

PES measurements were carried out in a commercial AXIS-ULTRA DLD spectrometer using an Al Kα (1486.6 eV) XPS source and a discharge UV lamp delivering photons at 21.2 eV corresponding to the He Iα line typically used in UPS. Under these conditions, the intrinsic spectral resolution was measured at the Fermi edge of the Ag foil at room temperature and estimated to be 0.15 eV. For comparison, the intrinsic resolution of a lab-based XPS setup using a monochromatized source is more than 0.55 eV. The UP spectral analysis was conducted using the Fermi level of Ag as internal calibration energy. Likewise, the background was corrected using a mathematical function developed by Li *et al.*,[21] (Figure S2) for UPS analysis and implemented later by Maheu *et al.*,[20] on TiO_2 nanopowders. After background subtraction, the signal was fitted by using a Gaussian function. In parallel, XPS analysis on CeO_2/Ag revealed well-resolved core levels corresponding to Ce 3d, C 1s, and Ag 3d. Ce 3d core levels were fitted using a combination of Voigt line shapes for Ce^{4+} and Ce^{3+}, including asymmetric shapes.

Temperature Programmed Reduction (TPR)

The reducibility of CeO_2 nanopowder was determined by TPR measurements (Figure S4) using a 9 Omnistar GSD 301 Pfeiffer Vacuum mass spectrometer. The dried sample (100 mg) was loaded into a suitable reactor and heated from room temperature to 600 °C (10 °C min^{-1}) for 4 h under 1%O_2/He to pre-treated CeO_2 and then cooled down to room temperature. Then, it was heated from room temperature up to 650 °C (10 °C min−1) under 1% H_2-Ar.

Results and discussion

The complexity of the Ce 3d core level fitting procedure requires a *prior* determination of the origin of each of its components, for which an XPS analysis on the polycrystalline model foil of ceria was executed under *in situ* oxidation conditions, starting from an almost fully reduced state (as outlined in the experimental section). Figure 2(a) shows the partial oxidation of polycrystalline ceria foil at low pressure (P_{ox}≈10^{-6} Torr). Each Ce 3d XPS spectrum was obtained over the same analysis zone while the surface $CeO_{2-\delta}$ was continuously oxidized, achieving thus nearly stoichiometric ceria. This *in situ* analysis allowed the identification of each of the components of the Ce 3d state linked to the transitions denoted with the labels $4f^0$, $4f^1$, and $4f^2$, as well as the presence of satellites and plasmons, which impact the fit (see arrows in Figure 2a). Although these transitions are known for single-crystal[22] and epitaxial growth ceria,[23] little is known about their behavior on an amorphous surface, as that of ceria in the form of powder.

The bottom of figure 2(a) describes the electronic transitions of the Ce 3d core level corresponding to the nearly fully reduced ceria surface ($CeO_{2-\delta}$), characterized by the missing of u''' and v''' components, corresponding to the $4f^0$ fundamental transitition of stoichiometric ceria. Instead, a mixture of the $4f^1$ and $4f^2$ transitions takes place, which are associated to v_0-u_0 and v'-u' components .

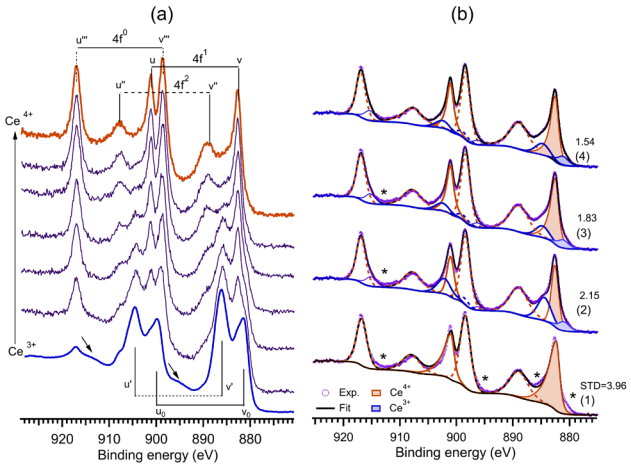

Fig. 2: (a) Core level (XPS) evolution. **Bottom:** Ce 3d spectrum (blue) corresponding to nearly-fully reduced ceria **foil** under Ar^+ sputtering. Arrows highlights the presence of plasmonic structures. Subsequently the eroded ceria foil was exposed to O_2 (P_{ox}≈10^{-6} Torr) under *in situ* conditions during XPS analysis, reaching a nearly-oxidized ceria at the **top** of the figure (red). (b) Ce 3d XPS analysis was carried out on nearly stoichiometric CeO_2 **nanopowders** after *in situ* oxidation O_2. Ceria nanopowder was pretreated in a catcell connected with the analysis chamber: (**1**) fitted with high asymmetric function located in v and u without Ce^{3+} contributions, (**2**) fitted combining Ce^{3+} and Ce^{4+} with only symmetric functions, (**3**) fitted with moderate asymmetric function located v and u and Ce^{3+} contributions, (**4**) fitted with moderate asymmetric function located v, u and v'' and u'' including Ce^{3+}

On the other hand, while the surface is continuously oxidized, the emergence of the electronic transition $4f^0$ is remarked,

concomitant with the evolution of the $4f^1$ and $4f^2$ transitions. This is evident on the spectrum at the top of figure 2(a), revealing the coexistence of all the electronic transitions ($4f^0$, $4f^1$, $4f^2$) related to multiplet effects coupling the spin and angular momentum of the f electron in the 3d core hole.[24] Furthermore, this mixed-valent state was confirmed by an electron 4f occupancy of about 0.6.[25] Therefore, as shown in Figure 2(a), the Ce 3d spectrum imposes a challenge for quantifying Ce^{3+} and Ce^{4+} species as it combines the presence of multiplet effects and mixed valence states.

To further complexify the Ce 3d spectral analysis, some additional structures (marked by arrows) observed at the bottom of Figure 2(a) on the nearly fully reduced ceria spectrum cannot be assigned to the effects mentioned above. Instead, these structures are attributable to collective electronic oscillations of plasmonic type.[23] However, under these low oxidative conditions (10^{-6} Torr), a high concentration of Ce^{3+} is expected, which could explain the coexistence of specific structures in the top spectrum Figure 2(a).

The absence of reliable methods of charge compensation for UPS analysis, such as those used during an XPS analysis (electron flood gun, pulsed ion gun),[26] precludes this type of solution for measuring the valence band on ceria foil by UPS. In this context, we applied a methodology developed in our previous research work[20] in order to minimize the charge effects during a UPS analysis. Ceria in nanopowder form was drop-casted on a cleaned silver foil, O 1s and C 1s core levels (See Figure 1, SI), confirming the absence of contamination. Moreover, the plasmonic structures located in the Ag 3d level and the Fermi level of Ag (Figure 3(a)) confirm the metallic character of treated Ag foil. Therefore, Fermi level, plasmons, and absence of O 1s and C 1s support the metallic character of the Ag foil. Thus, the drop-casted $CeO_{2-\delta}$/Ag was oxidized in an *in situ* reaction catcell (catalytic reaction chamber) to obtain nearly stoichiometric ceria free of impurities and artifacts. This surface was analytically evaluated by combining asymmetric and symmetric functions, as observed in Figure 2(b). At the bottom (1), the spectrum of Ce 3d corresponds to fully oxidized *in situ* ceria. To fit this spectrum, in addition to the complexity introduced by the number and position of components, a certain degree of asymmetry must be imposed to fit this with an acceptable standard deviation of the residual values (STD). It is known that the shape of the peak depends on the inverse of the lifetime of the photo-electro-generated core-hole.[27] *A priori*, the carrier lifetime of ceria is about 1.52 ns,[28] which justifies the use of specific asymmetrical peak shapes in ceria. However, the debate still exists regarding the level of peak asymmetry. Some authors propose asymmetric peaks only in the $4f^1$ transition,[6,29] while others propose to impose an asymmetry on the $4f^2$ transition.[24] The discussion of asymmetry extends even to the type of function to be used by proposing an analysis of Ce 3d based on Doniach-Sunjic (DS) lineshapes[30] but with an asymmetric parameter $\alpha = 0$, reducing DS lineshape to a Lorentzian function.[27] This choice is because DS is a fit function, which follows the relaxation of electron-hole excitation, particularly the relaxation of the electron conduction gas in metallic systems.[31] Therefore, it does not apply to insulators such as CeO_2. In this context, the oxidized Ce 3d was fitted using a Lorentzian function whose asymptotic form is equivalent to the asymptotic form of the theoretical DS asymmetric lineshape.

Several fits were executed in Figure 2(b): (**1**) was performed with an asymmetric function on v and u peaks without including any Ce^{3+} related components. This fit has a poor STD (3.96), where the regions marked with asterisks show the absence of spectral weight. (**2**) The fit was performed regardless of asymmetric peak shapes but included the components associated with Ce^{3+}, the atomic concentration of Ce^{3+} here is approx. 25%. In (**3**) with a moderate asymmetry on v and u, the concentration of Ce^{3+} decreases to 18%, while (**4**) with moderate asymmetries in v, u and v'', u'' the concentration of Ce^{3+} is about 19%. Therefore, in this scenario, asymmetric lineshapes become a controversial adjusting parameter, usually used to reach a better fit. This analysis shows that regardless of the degree of asymmetry introduced, the Ce^{3+} contribution is required in order to fit the spectrum, which should be at least 18%.

By this Ce 3d core level analysis, we want to highlight the complexity of the fit procedure, which is quite ambiguous[5,6,24,30]. For instance, Allahgholi *et al.*,[23] have evoked the ambiguity of factor analysis procedure proposed by Holgado *et al.*,[5] essentially due to the presence of satellites in the Ce^{3+} contribution, which impact the Ce 3d shape. To date, resonant photoemission remains the most appropriate method for monitoring the Ce^{3+} and Ce^{4+} states.[32] However, tunable soft-x-rays are required, and photolysis effects cannot be excluded either.

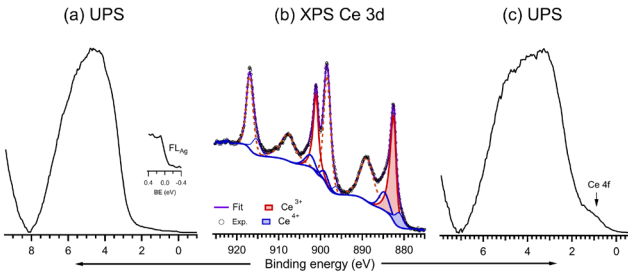

Fig. 3: (a) Valence band (UPS) after *in situ* oxidation and before XPS analysis. (b) Ce 3d core level of *in situ* oxidized CeO_2 nanopowders after UPS. (c) UPS analysis on oxidized ceria after XPS analysis. The arrow points on the Ce 4f state. Insert: reminiscent Ag_{FL}

Figure 3(a) shows the UP HeI valence band spectrum of *in situ* oxidized ceria, which exhibits a stochiometric character mainly due to a large band formed mainly by O 2p orbitals with ≈ 4 eV broad. It corresponds to a position of the valence band maximum located at ≈ 2.5 eV below the Fermi level of Ag foil. The UP spectral analysis on stoichiometric semiconducting ceria was carried out using the Fermi level of Ag as internal calibration energy.[20,26] The bandwidth and bandgap (Eg)

parameters are in line with those reported in previous experimental[33,34] and theoretical studies.[16,35] It is crucial to note that from an experimental point of view, the stoichiometric character of oxidized ceria is associated with the absence of the Ce 4f state located between 1.5 eV and 1.9 eV, this feature, in conjunction with a valence band maximum measured to ≈2.5 eV below the Fermi level reveals the valence band of CeO_2 - Ce 4f(0) as reported in the literature for ultra-thin model films of ceria.[6,33] Following the analysis sequence, an XPS Ce 3d level spectrum of on *in situ* oxidized ceria reveals six visible components containing five $3d_{5/2}$-$3d_{3/2}$ spin-orbit-split doublets fitted according to the method proposed on the spectrum (**4**) Figure 2(b). This class of multi-doublet XPS spectrum is challenging to adjust due to complex final states and electron-hole perturbations. However, from figure 3(b) one can identify the spectral weight associated to Ce^{3+} at 881.0 eV and 884.6 eV for Ce $3d_{5/2}$ accompanied with 899.2 eV and 902.2 eV for Ce $3d_{3/2}$. Surprisingly, the concentration of Ce^{3+} on pre-oxidized ceria is relatively high, revealing 19% of Ce^{3+} with an STD = 1.54. Several theoretical studies suggest the coexistence of Ce^{3+} and Ce^{4+} with 4fn (with n approx. 0.5) in most samples,[25,36,37] which could be related to the nano-size of CeO_2 particles and the surface/bulk dependence of the Ce^{3+}/Ce^{4+} ratio.[38]

A subsequent UPS analysis on oxidized ceria verified this discrepancy in Figure 3(c), highlighting a new state close to the Fermi level at ≈1.6 eV. This state is characteristic of sub-stoichiometric ceria $CeO_{2-\delta}$ with a state Ce 4f. Its presence is concomitant with a modification between 2 eV and 8 eV where O 2p hybridized orbitals are located, revealing structural changes associated with oxygen atoms.

Discrepancies between UPS analysis before and after XPS reveal the photoreductive effect induced by X-rays on ceria, contrary to UPS. The magnitude of the Ce 4f state depends on various parameters such as (i) beam exposure time, (ii) power of the X-ray source, (iii) surface treatments, (iv) the intrinsic nature of the material (including the size of particles, electronic configuration) and (v) power density (PD) of the beam.[9] PD is a critical parameter used to estimate the impact of a beam source on a surface (photolysis/beam-damage), as this parameter represents the power received on the surface of the sample per unit area. For instance, at a similar photon flux (ϕ), the power density (PD =ϕ(hc/λ)) induced by the X-rays is one order of magnitude higher than that generated by a UV source at 21.2 eV (UPS) of incident energy. Indeed, other parameters as those mentioned in (iv) should not be underestimated. For instance, the literature reports X-ray beam reduction on other oxides after XPS analysis, such as MoO_3.[39,40] Highlighting that X-ray beam damage is not specific to ceria. All these effects can influence the quantification of Ce^{3+} through XPS. Therefore special care must be taken in the use of the XPS technique as it contributes to an over-estimation of the Ce^{3+} concentration at the surface of ceria induced by photoreduction. This analysis highlights that UPS must be established as a "routine" technique to estimate the Ce^{3+} surface concentration on ceria nanopowders, as this spectroscopy exerts a lower degree of photoreduction on the surface of ceria and a straightforward interpretation *via* the Ce 4f orbital located at the extreme surface.

Although it is assumed that Ce^{3+} cations are located at the surface, their detection will depend on the depth of the analysis. Therefore, it is expected that following an *in situ* reduction, the surface of ceria will be densely populated by Ce^{3+} cations. Following this strategy, post-analyzed stoichiometric ceria was reduced under ultra-high vacuum (UHV) at 600 °C and characterized *in situ*. UPS analysis revealed the evolution of the electronic structure before and after reduction (Figure 4(a), (b)), which is concomitant with the presence of an intense Ce 4f state located at ≈ 1.4 eV (arrow) and also with a significant change of color of the sample (see the picture in Figure 4(c): insert). XPS confirms the surface-reduction dependence with a modest increase to 26% (Figure 4(c,d)) for post-reductive ceria versus 19% after UPS-XPS analysis on post oxidative treatment, a mere 7% over oxidized ceria.

Although the UPS data presented in this paper allows a qualitative approximation of the evolution of the Ce^{3+}/Ce^{4+} ratio, the UPS uses is limited as this requires the development of quantitative methods. An alternative would be to get a sample reference totally reduced (Ce_2O_3). However, it is not apparent to get a pure Ce_2O_3 sample (without metallic Ce) by reduction at high temperature, as the reduction rate not only depends on temperature[41] Furthermore, compounds

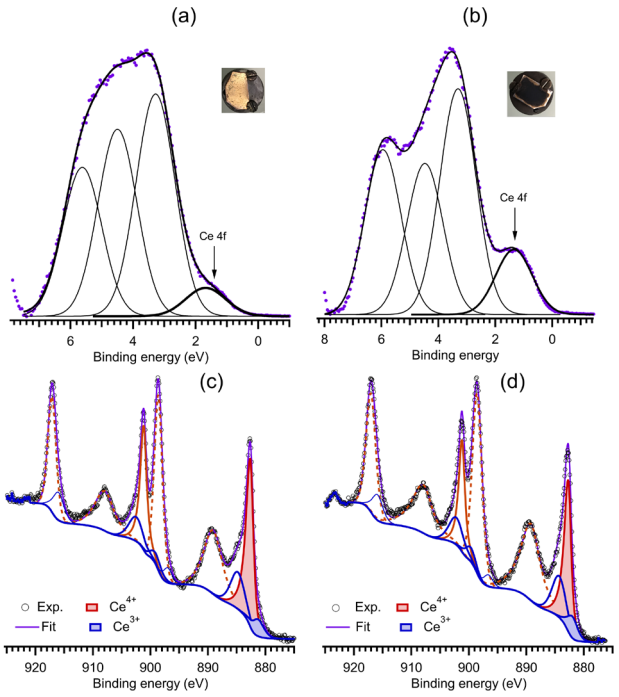

Fig. 4: (a) UPS spectrum on *in situ* oxidized ceria (600 °C under O_2) after XPS analysis fitted by four main components. (c) XPS on *in situ* oxidized ceria after UPS analysis. (b) UPS fitted by four main components and (d) XPS analysis on reduced ceria (600 °C under UHV). Insert: Photo of oxidized ceria (left) and reduced (right), respectively.

containing 100% of Ce^{3+} cations such as $CeCl_3$ or cerium nitrate contain orbitals that interfere with O 2p and Ce 4f in the valence band region.

To carry out a quantitative analysis to determine the Ce^{3+}/Ce^{4+} ratio without a reference sample would require several hypotheses to be fulfilled: (i) Hybridization between Ce 4f, Ce 5d, and O 2p orbitals is negligible. Theoretical calculations propose a strong ionic character for stoichiometric CeO_2 and sub-stoichiometric $CeO_{2-\delta}$ concomitant with a low orbital overlap in the O 2p region located in the valence band.[16,18,19] The density of states (DOS) of Ce 4f and Ce 5d inside the O 2p region is extremely low, generally associated with electronic tails or reminiscent states, giving it a strong O 2p character to CeO_2 and $CeO_{2-\delta}$. However, this is valid only from a theoretical point of view, as an increase in intensity will be observed if these theoretical states are normalized by the experimental photoionization cross-section (PICS) at 21.2 eV. This explains the shape evolution before and after reduction between 8 and 3 eV in the UPS spectra (see Figure 4(a) and (b)). (ii) Be aware of the true photoionization cross-section values and not approximated values. Since the literature does not provide photoionization cross-section data for sub-stoichiometric ceria (mixed Ce^{3+} and Ce^{4+}, data available only for neutral ceria atoms), the quantitative concentration obtained is not entirely reliable, although their trend is undoubtedly correct.

Despite these limitations, an analytical procedure was carried out on the valence band UPS spectrum of ceria after XPS analysis (Figure 4(a)) and post-reductive treatment (Figure 4(b)), respectively. In both spectra, the subtraction of background was carried out by using the function developed by Li *et al*.[21] As proposed by Maslakov *et al*.[17,42] the valence band can be adjusted with several components, and the number of fit contributions is limited by the resolution of the technique either ≈0.6 eV for XPS and ≈0.2 eV for UPS[20]. In order to determine the area of the O 2p region (2 and 8 eV) and Ce 4f (≈1.6 eV), four Gaussian contributions were applied to adjust the valance band region (O 2p and Ce 4f). Although a UP signal renormalization derived from the PICS may provide a way to quantify Ce^{3+}/Ce^{4+}, this approach is limited as this method requires valid photoionization cross-section values corresponding to ionized ceria ($CeO_{2-\delta}$). Since the literature does not provide such data for sub-stoichiometric ceria, the quantitative concentration obtained would not be reliable. However, this does not preclude a relative comparison of the O 2p and Ce 4f areas as substoichiometric ceria has a strong ionic character. From Figures 4 (a) and (b), one can verify the relative area increment corresponding to the Ce 4f state, which is doubled after *in situ* reduction, confirming the effects of surface reduction higher than those observed by XPS. It is worth noting that the presence of oxygen contamination is negligible as all the preparation was carried out *in situ* without exposing the sample to the air during the transfer. Although this methodology should be taken with caution and only as a starting point toward developing a robust method combining DFT, PICS calculations, and UPS analysis, it should be noted that UPS is sensitive to the outermost surface, giving access to Ce^{3+} cations after reduction. In addition, TPR analysis, a bulk technique, was carried out in severe conditions to get an extreme value, which revealed only 2.8% of Ce^{3+} after reduction at 600 °C under H_2 flow (see Figure S4 in SI). This Ce^{3+} value is much lower than the one obtained by UPS, confirming that ceria reduction is mainly happening at the surface, in agreement with the literature.[4] This low value compared to that deduced from UPS after reduction at 600 °C in UHV can be explained by the penetration depth of UPS (≈ 5 Å), which is much lower than the crystallite size of CeO_2 (32 nm, see Figure S3 in SI) and preferential reduction of ceria at the surface leading to a Ce^{3+} concentration gradient from the surface to the bulk.

Conclusions

To conclude, we have analyzed the electronic structure of stoichiometric and sub-stoichiometric ceria in the form of nanopowders by UPS and XPS spectroscopies under *in situ* conditions. A sequential analysis of UPS→XPS highlighted the overestimation of the reduction rate (Ce^{3+}) obtained by XPS and the photoreduction effect during XPS analysis. XPS revealed a low evolution of Ce^{3+} concentration before (19%) and after reductive treatment (26%), highlighting thus that photolysis contribution is major. UPS confirmed this photolysis effect by detecting Ce^{3+} induced by the X-ray beams. We have demonstrated by UPS the high degree of reduction (doubled of Ce^{3+}) at the outermost surface of ceria after reductive treatment at 600 °C. Therefore, a photoemission analysis under low power density flux UPS at 21.2 eV allows qualitatively estimating the rate of Ce^{3+} at the outermost surface of ceria subjected to different oxidative and reductive treatments and *in situ* reaction conditions.

Conflicts of interest

There are no conflicts to declare.

Acknowledgement

C. M. acknowledges the French Ministry of Education for the financial support of his Ph.D. thesis.

Notes and references

‡ Footnotes relating to the main text should appear here. These might include comments relevant not central to the matter under discussion, limited experimental and spectral data, and crystallographic data.

§

§§

1 T. Montini, M. Melchionna, M. Monai and P. Fornasiero, Fundamentals and Catalytic Applications of CeO_2-Based Materials, *Chem. Rev.*, 2016, **116**, 5987–6041.

2 E. Aneggi, D. Wiater, C. de Leitenburg, J. Llorca and A. Trovarelli, Shape-Dependent Activity of Ceria in Soot Combustion, *ACS Catal.*, 2014, **4**, 172–181.

3 E. Paparazzo, Use and mis-use of x-ray photoemission spectroscopy Ce3d spectra of Ce_2O_3 and CeO_2, *J. Phys.: Condens. Matter*, 2018, **30**, 343003.

4 S. Kato, M. Ammann, T. Huthwelker, C. Paun, M. Lampimäki, M.-T. Lee, M. Rothensteiner and J. A. van Bokhoven, Quantitative depth profiling of Ce^{3+} in Pt/CeO_2 by in situ high-energy XPS in a hydrogen atmosphere, *Phys. Chem. Chem. Phys.*, 2015, **17**, 5078–5083.

5 J. P. Holgado, R. Alvarez and G. Munuera, Study of CeO_2 XPS spectra by factor analysis: reduction of CeO_2, *Applied Surface Science*, 2000, **161**, 301–315.

6 T. Skála, F. Šutara, K. C. Prince and V. Matolín, Cerium oxide stoichiometry alteration via Sn deposition: Influence of temperature, *Journal of Electron Spectroscopy and Related Phenomena*, 2009, **169**, 20–25.

7 E. Paparazzo, XPS studies of damage induced by X-ray irradiation on CeO_2 surfaces, *Surface Science*, 1990, **234**, L253–L258.

8 E. Paparazzo, G. M. Ingo, and N. Zacchetti, X-ray induced reduction effects at CeO_2 surfaces: An x-ray photoelectron spectroscopy study, *Journal of Vacuum Science & Technology A: Vacuum, Surfaces, and Films*, 1998, **9**, 1416.

9 J. El Fallah, L. Hilaire, M. Roméo and F. Le Normand, Effect of surface treatments, photon and electron impacts on the ceria 3d core level, *Journal of Electron Spectroscopy and Related Phenomena*, 1995, **73**, 89–103.

10 P. W. Park and J. S. Ledford, Effect of Crystallinity on the Photoreduction of Cerium Oxide: A Study of CeO_2 and Ce/Al_2O_3 Catalysts, *Langmuir*, 1996, **12**, 1794–1799.

11 F. Zhang, P. Wang, J. Koberstein, S. Khalid and S.-W. Chan, Cerium oxidation state in ceria nanoparticles studied with X-ray photoelectron spectroscopy and absorption near edge spectroscopy, *Surface Science*, 2004, **563**, 74–82.

12 T.-S. Wu, L.-Y. Syu, S.-C. Weng, H.-T. Jeng, S.-L. Chang and Y.-L. Soo, Defect engineering by synchrotron radiation X-rays in CeO_2 nanocrystals, *Journal of Synchrotron Radiation*, 2018, **25**, 1395–1399.

13 C. T. Nottbohm and C. Hess, Investigation of ceria by combined Raman, UV–vis and X-ray photoelectron spectroscopy, *Catalysis Communications*, 2012, **22**, 39–42.

14 S. Loridant, Raman spectroscopy as a powerful tool to characterize ceria-based catalysts, *Catalysis Today*, 2021, **373**, 98–111.

15 M. Daniel and S. Loridant, Probing reoxidation sites by *in situ* Raman spectroscopy: differences between reduced CeO_2 and Pt/CeO_2, *Journal of Raman Spectroscopy*, 2012, **43**, 1312–1319.

16 M. E. Khalifi, F. Picaud and M. Bizi, Electronic and optical properties of CeO_2 from first principles calculations, *Anal. Methods*, 2016, **8**, 5045–5052.

17 K. I. Maslakov, Y. A. Teterin, M. V. Ryzhkov, A. J. Popel, A. Y. Teterin, K. E. Ivanov, S. N. Kalmykov, V. G. Petrov, P. K. Petrov and I. Farnan, The electronic structure and the nature of the chemical bond in CeO_2, *Phys. Chem. Chem. Phys.*, 2018, **20**, 16167–16175.

18 A. Pedrielli, P. de Vera, P. E. Trevisanutto, N. M. Pugno, R. Garcia-Molina, I. Abril, S. Taioli and M. Dapor, Electronic excitation spectra of cerium oxides: from ab initio dielectric response functions to Monte Carlo electron transport simulations, *Phys. Chem. Chem. Phys.*, 2021, **23**, 19173–19187.

19 N. V. Skorodumova, R. Ahuja, S. I. Simak, I. A. Abrikosov, B. Johansson, and B. I. Lundqvist, Electronic, bonding, and optical properties of CeO_2 and Ce_2O_3 from first principles, *Phys. Rev. B*, 2001, **64**, 115108.

20 C. Maheu, L. Cardenas, E. Puzenat, P. Afanasiev and C. Geantet, UPS and UV spectroscopies combined to position the energy levels of TiO_2 anatase and rutile nanopowders, *Phys. Chem. Chem. Phys.*, 2018, **20**, 25629–25637.

21 X. Li, Z. Zhang and V. E. Henrich, Inelastic electron background function for ultraviolet photoelectron spectra, *Journal of Electron Spectroscopy and Related Phenomena*, 1993, **63**, 253–265.

22 C. Barth, C. Laffon, R. Olbrich, A. Ranguis, P. Parent and M. Reichling, A perfectly stoichiometric and flat CeO_2(111) surface on a bulk-like ceria film, *Sci Rep*, 2016, **6**, 21165.

23 A. Allahgholi, J. I. Flege, S. Thieß, W. Drube and J. Falta, Oxidation-State Analysis of Ceria by X-ray Photoelectron Spectroscopy, *ChemPhysChem*, 2015, **16**, 1083–1091.

24 F. Le Normand, J. El Fallah, L. Hilaire, P. Légaré, A. Kotani and J. C. Parlebas, Photoemission on 3d core levels of Cerium: An experimental and theoretical investigation of the reduction of cerium dioxide, *Solid State Communications*, 1989, **71**, 885–889.

25 A. Fujimori, Mixed-valent ground state of CeO_2, *Phys. Rev. B*, 1983, **28**, 2281–2283.

26 J. W. Kim and A. Kim, Absolute work function measurement by using photoelectron spectroscopy, *Current Applied Physics*, 2021, **31**, 52–59.

27 G. K. Wertheim and S. B. Dicenzo, Least-squares analysis of photoemission data, *Journal of Electron Spectroscopy and Related Phenomena*, 1985, **37**, 57–67.

28 M. Li, P. Wang, Z. Ji, Z. Zhou, Y. Xia, Y. Li and S. Zhan, Efficient photocatalytic oxygen activation by oxygen-vacancy-rich CeO_2-based heterojunctions: Synergistic effect of photoexcited electrons transfer and oxygen chemisorption, *Applied Catalysis B: Environmental*, 2021, **289**, 120020.

29 T. Skála, F. Šutara, M. Škoda, K. C. Prince and V. Matolín, Palladium interaction with CeO_2, Sn–Ce–O and Ga–Ce–O layers, *J. Phys.: Condens. Matter*, 2008, **21**, 055005.

30 M. Romeo, K. Bak, J. El Fallah, F. Le Normand and L. Hilaire, XPS Study of the reduction of cerium dioxide, *Surface and Interface Analysis*, 1993, **20**, 508–512.

31 S. Doniach and M. Sunjic, Many-electron singularity in X-ray photoemission and X-ray line spectra from metals, *J. Phys. C: Solid State Phys.*, 1970, **3**, 285–291.

32 V. Matolín, I. Matolínová, L. Sedláček, K. C. Prince and T. Skála, A resonant photoemission applied to cerium oxide based nanocrystals, *Nanotechnology*, 2009, **20**, 215706.

33 A. Pfau and K. D. Schierbaum, The electronic structure of stoichiometric and reduced CeO_2 surfaces: an XPS, UPS and HREELS study, *Surface Science*, 1994, **321**, 71–80.

34 D. R. Mullins, S. H. Overbury and D. R. Huntley, Electron spectroscopy of single crystal and polycrystalline cerium oxide surfaces, *Surface Science*, 1998, **409**, 307–319.

35 P. J. Hay, R. L. Martin, J. Uddin and G. E. Scuseria, Theoretical study of CeO_2 and Ce_2O_3 using a screened hybrid density functional, *J. Chem. Phys.*, 2006, **125**, 034712.

36 E. Shoko, M. F. Smith and R. H. McKenzie, Mixed valency in cerium oxide crystallographic phases: Valence of different cerium sites by the bond valence method, *Phys. Rev. B*, 2009, **79**, 134108.

37 A. Kotani, T. Jo and J. C. Parlebas, Many-body effects in core-level spectroscopy of rare-earth compounds, *Advances in Physics*, 1988, **37**, 37–85.

38 C. Paun, O. V. Safonova, J. Szlachetko, P. M. Abdala, M. Nachtegaal, J. Sa, E. Kleymenov, A. Cervellino, F. Krumeich and J. A. van Bokhoven, Polyhedral CeO_2 Nanoparticles: Size-Dependent

Geometrical and Electronic Structure, *J. Phys. Chem. C*, 2012, **116**, 7312–7317.

39 X. Liao, A. R. Jeong, R. G. Wilks, S. Wiesner, M. Rusu and M. Bär, X-ray irradiation induced effects on the chemical and electronic properties of MoO3 thin films, *Journal of Electron Spectroscopy and Related Phenomena*, 2016, **212**, 50–55.

40 J. Baltrusaitis, B. Mendoza-Sanchez, V. Fernandez, R. Veenstra, N. Dukstiene, A. Roberts and N. Fairley, Generalized molybdenum oxide surface chemical state XPS determination via informed amorphous sample model, *Applied Surface Science*, 2015, **326**, 151–161.

41 S. Ackermann, L. Sauvin, R. Castiglioni, J. L. M. Rupp, J. R. Scheffe and A. Steinfeld, Kinetics of CO2 Reduction over Nonstoichiometric Ceria, *J. Phys. Chem. C*, 2015, **119**, 16452–16461.

42 K. I. Maslakov, Y. A. Teterin, A. J. Popel, A. Yu. Teterin, K. E. Ivanov, S. N. Kalmykov, V. G. Petrov, P. K. Petrov and I. Farnan, XPS study of ion irradiated and unirradiated CeO2 bulk and thin film samples, *Applied Surface Science*, 2018, **448**, 154–162.